Journal of Materials Chemistry A

Accepted Manuscript

ROYAL SOCIETY OF CHEMISTRY

www.rsc.org/materialsA

Journal of Materials Chemistry A RSC Publishing

ARTICLE

Growth of Ni-Co binary hydroxide on reduced graphene oxide surface by a successive ionic layer adsorption and reaction (SILAR) method for high performance asymmetric supercapacitor electrode

Cite this: DOI: 10.1039/xoxxoooooox

Received ooth January 2012,
Accepted ooth January 2012

DOI: 10.1039/xoxxoooooox

www.rsc.org/

Milan Jana,[a,b] Sanjit Saha,[a,b] Pranab Samanta,[a] Naresh Chandra Murmu,[a] Nam Hoon Kim,[c] Tapas Kuila*[a] and Joong Hee Lee*[c]

A simple, additive-free, cost-effective and scalable successive ionic layer adsorption and reaction (SILAR) method is reported to prepare nickel-cobalt binary hydroxide (Ni-Co-BH) on reduced graphene oxide (RGO) directing template over a macro porous conductive nickel foam substrate. This green technique is not only considered as fundamental research interest, but also describes the commercial applications of supercapacitors to reduce the electrode fabrication cost. Three different Ni-Co-BH-G (Ni-Co-BH/RGO) composites are synthesised by tailoring the nickel-cobalt ratios. The flower like 3 D framework of Ni-Co-BH-G provides a porous nano structure to facilitate the charge transfer and ion diffusion. The cathodic peak current density vs. square root of the scan rate slope values of cyclic voltammetry are consistent with specific capacitance (SC) retention (vs. current density) from charge-discharge curves and the diffusion time constant of the Nyqusit plot of the Ni-Co-BH-G composites. Taking the advantage of 3 D conductive meso porous open framework, the Ni-Co-BH-G has provided excellent SC of 2130 F g^{-1} at 2 A g^{-1}. An asymmetric supercapacitor device is designed with the optimized Ni-Co-BH-G as positive electrode and concentrated HNO_3 treated conducting carbon cloth (CCN) as the negative electrode. An excellent energy density of ~92 W h kg^{-1} and high power density of ~7.0 kW kg^{-1} with lifetime stability up to 10,000 charge-discharge cycles (capacitance retention ~80%) is provided by the asymmetric device. Four asymmetric devices have been assembled in a series, which provided ~5.6 V charge-discharge potential. The assembled system has powered a 5 V light-emitting diode (LED) successfully.

1. Introduction

Design of exceedingly efficient energy storage devices with elevated power and energy output and extended life span is required urgently for the proper utilization of renewable energy sources to fulfil the rising energy demand considering the environmental issues (e.g. with low CO_2 emission).[1-5] Supercapacitors are emerging as the supplement to batteries; provide distinctive advantages such as short charging time, safe operation mode and high power density.[1-5] Currently, supercapacitors suffer from limited energy density in comparison to rechargeable lithium ion batteries.[1-6] In recent years, enormous research efforts have been made to engineer high energy density supercapacitor devices with nano-structured electrode materials.[4-12] Carbon-based materials (carbon nanotubes, graphene, etc.), conducting polymers (poly aniline, poly pyrrole, polythiophene etc.), and transition metal oxide/hydroxide have been investigated more intensively for supercapacitor applications.[4-12] Supercapacitors using carbon based materials provide surface-dominant low specific capacitance through electrical double layer (EDL) mechanism.[13-15] Owing to their faradic energy storage mechanism conducting polymers, transition metal oxide/hydroxide exhibited elevated specific capacitance.[9-12] However, the supercapacitor applications of these electrode materials are limited due to the poor electrical conductivity and low electrochemical stability.[16-20] Therefore, the development of novel materials with high electrical conductivity, large specific capacitance and long term cyclic stability is very important in supercapacitor research. A single component can rarely afford all of these distinct characteristics. Recent literatures in nanotechnology have enabled colossal promises to prepare multi functional composite materials with different nano-architecture.[21-27] Various binary/ternary composites have been investigated with significant advantages over single component.[21-27] Hsu et al. reported a mesoporous $NiCo_2O_4$ composite with a specific capacitance of 764 F g^{-1} at 2 mV s^{-1}. The asymmetric cell based on the mesoporous $NiCo_2O_4$ composite exhibited an energy and power density of 17.72 W h kg^{-1} and 25.42 kW kg^{-1}, respectively.[21] Wang et al. reported a facile route to prepare mesoporous Ni-Co binary oxide nano-sheets by the "formation and dissociation" of citrate complex with a high

specific capacitance of 1846 F g^{-1} in three electrode system.[22] The designed asymmetric cell based on the Ni-Co binary oxide explored an energy density of 71.7 W h kg^{-1} with an elevated power density of 400 W kg^{-1}. A nano honeycomb like $CoMoO_4$-3D graphene composite was reported by Yu et al. with an energy density of 21.1 W h kg^{-1} at a power density of 300 W kg^{-1}.[23] The high temperature annealing for the conversion of metal hydroxide/carbonate to oxide may create defects to the surface and reduce the hydrous part causing deterioration of the supercapacitor properties of metal oxides as compared to their metal hydroxides.[24,28-30] Recently, binary metal hydroxides have also been explored as supercapacitor electrode materials.[29-31] Tang et al. engineered floss like Ni-Co binary hydroxide over sodium dodecyl benzene sulfonate template and the composite exhibited a specific capacitance of 918.9 F g^{-1} (at 0.2 A g^{-1}).[29] Sun et al. explored the morphology dependent Ni-Co binary hydroxide composite as supercapacitor electrode materials with energy density of 26.3 W h kg^{-1} at a power density of 320 W kg^{-1}.[30] A zinc tin oxide nanowires supported Ni-Co layer double hydroxide was demonstrated by Wang et al. with an energy density of 23.7 W h kg^{-1} at a power density of 284.2 W kg^{-1}.[31] However, these binary metal hydroxide cannot be used directly as supercapacitor electrode due to their poor electrical conductivity and lack of adhesion. Therefore, the use of conductive filler (carbon black, acetylene black) and non-conducting binder (Polyvinylidene fluoride, Polytetrafluoroethylene, etc.) is a common practice to fabricate the supercapacitor electrodes.[29-31]The use of non conducting binders deteriorates electrochemical properties providing "dead surface" in the electrochemical charge-storage route.[32] In order to avoid the "dead surface", design of binder and additive free electrodes is the key point in the supercapacitor research.[32-35] Patil et al. described a two step method to develop Co-Ni hydroxides over 3 D graphene foam.[36] The composite materials prepared by chemical vapour deposition (CVD) and chemical bath deposition (CBD) provided a specific capacitance of 1847 F g^{-1} at a current density of 5 A g^{-1}. A binder-free 3 D binary Ni-Co hydroxide/graphene/nickel foam electrode was developed by CVD combined with electrochemical deposition (ED) method.[37] However, the materials developed by CVD, CBD and ED are not suitable for the fabrication of low cost and high performing supercapacitor device. Herein, Ni-Co binary hydroxide (Ni-Co-BH) composite was developed over reduced graphene oxide (RGO) template, where nickel foam (NF) was used as substrate by a "successive ionic layer adsorption and reaction" (SILAR) method. The SILAR method plays with ions instead of atoms, resulting layer by layer assembly of Ni-Co-BH and RGO (Ni-Co-BH-G), which offers an excellent electrochemical path to boost the supercapacitor properties.[33-35]The Ni-Co-BH-G deposited on NF was directly used as supercapacitor electrode. The film thickness of Ni-Co-BH-G composite on NF can be controlled with number of cycles. The Ni-Co-BH-G exhibited very high specific capacitance of 2130 F g^{-1} at a current density of 2 A g^{-1} in three electrode measurement. The designed asymmetric device with the Ni-Co-BH-G as positive electrode and nitric acid treated carbon cloth (CCN) as negative electrode material exhibited an energy density of ~92 W h kg^{-1} and high power density of 7.0 kW kg^{-1}.

2. Experimental

2.1 Materials

Commercial flake graphite was purchased from M/s Graphite & Mineral Products, Kolkata, India. Sulphuric acid, Hydrochloric acid, hydrogen peroxide, potassium permanganate and potassium hydroxide and sodium hydroxide, N, N-dimethyle formamide (DMF) were obtained from Merck, Mumbai, India. Cobalt chloride and nickel chloride were purchased from SRL, Mumbai, India. NF and conducting carbon cloth (CC) were obtained from Shanghai Winfay New Material Co., Ltd, China and Flips India Engineering, Mumbai-400093, India, respectively. Polyvinylidene fluoride (PVDF) was purchased from Sigma Aldrich. Stainless steel (SS) of ~ 0.2 mm thickness was purchased from a local market of Durgapur, India.

2.2 Synthesis of Ni-Co-BH-G

Ni-Co-BH-G composites were fabricated onto the flexible NF (20×20 mm^2) substrate through the immersion of NF in alternating graphene oxide (GO) dispersion and metal salt bath (source of Ni^{2+} and Co^{2+} ions). Five-beaker (100 ml) system (SILAR) was employed to grow the Ni-Co-BH/G composite over NF. About 80 ml of GO dispersion (1 mg ml^{-1}) was taken in the 1st beaker. The graphite oxide was prepared by modified Hummer's method as discussed earlier.[32] The measured amount (~80 mg) of graphite oxide was exfoliated in 80 ml of deionised water (DI) water through 30 min of water bath sonication. The dispersion was then centrifuged at ~6000 rpm to remove the un-exfoliated graphite/graphite oxide particles and the stable brown dispersion of GO was collected in the 1st beaker. The 2nd beaker contained the mixed metal chloride solutions of nickel chloride and cobalt chloride. About 80 ml 0.2 (M) NaOH solution was taken in 4th beaker. The 3rd and 5th beakers contained DI water. The NF was dipped in every dispersion/solutions for ~10 minutes one by one up to 20 mm by a programmable multi vessel dip coating unit (Xdip-MVI, Apex Instruments Co. Pvt. Ltd., Kolkata, India). In between every immersion the NF was kept to dry for ~10 minutes. The cycle was repeated for 3 times to achieve thicker coating of Ni-Co-BH-G on NF surface. The obtained Ni-Co-BH-G coated NF was dried overnight at ~60 ºC. Three different Ni-Co-BH/G composites were prepared; where the mixed metal salt solution contained 0.1 (M) $NiCl_2.6H_2O$ with different concentration of $CoCl_2.6H_2O$ (0.1, 0.2 and 0.4 M) resulting in the obtained products with names Ni-Co-BH-G1, Ni-Co-BH-G2 and Ni-Co-BH-G3, respectively. About 1 mg of Ni-Co-BH-G was deposited on NF after 3 numbers of cycles. For comparison, Ni-Co-BH based electrode was prepared following the same procedure in absence of GO. The precursor Ni-Co ratio was 1:1 for the synthesis of Ni-Co-BH electrode.

2.3 Synthesis of nitric acid treated carbon cloth (CCN)

The CC was chopped into fine pieces and sonicated for ~ 30 min with concentrated nitric acid followed by repeated washing with DI water. The nitric acid treated CC was heated at ~450º C for 30 min and designated as CCN.

2.4Fabrication of Ni-Co-BH/G//CCN asymmetric supercapacitor

Ni-Co-BH-G2//CCN asymmetric supercapacitor cell (2.0×2.0 cm^2) was fabricated by taking Ni-Co-BH-G2 coated NF as positive electrode and CCN as negative electrode material, respectively, where 6 (M) KOH was used as electrolyte and whatman 42 filter paper as dielectric separator. The CCN was not self supported to be used as supercapacitor electrode. The measured amount of CCN was mixed with ~10% PVDF and dispersed in DMF. The slurry was casted on 2×2 cm^2 SS (0.2 mm thickness) and dried in vacuum at 50 ºC. The designed cell was sealed into a plastic bag to avoid electrolyte evaporation during the long-time analysis.

3.1 Material characterization

Fourier transform infrared spectra (FT-IR) of Ni-Co-BH-Gs were recorded by Spectrum 100 FT-IR, PerkinElmer, USA. X-ray diffraction (XRD) of the samples was measured at room temperature by a D/Max 2500 V/PC (Rigaku Corporation,

Tokyo, Japan) at a scan rate of 1° min^{-1}. Raman spectroscopy of the samples was analysed with Nanofinder 30 (Tokyo Instruments Co., Osaka, Japan) with Laser wavelength of 514 nm and 100 μm spot size. The chemical composition and state of the composite were confirmed by X-ray photo electron spectroscopy (XPS) using axis-Nova, Kratos Analytical Ltd, Manchester, UK. The morphologies of the Ni-Co-BH-Gs were recorded by field-emission scanning electron microscopy (FE-SEM, Sigma HD, Carl Zeiss, Germany). The transmission electron microscopy (TEM) of Ni-Co-BH-G2 was measured using JEM-2100 FS (JEOL, Japan). The electrical conductivity of the samples was analysed by four probe method in a KEITHLEY (USA) delta arrangement consisting of AC and DC current source, model: 6221 and nanovoltmeter, model: 2182A using the formula $Conductivity = \frac{1}{4.53 \times R \times d}$ (1)

Where, R is the resistance and d (metre) is the thickness of the pellet.

3.2 Electrochemical measurements

The electrochemical tests were carried out in both three-electrode and two-electrode configurations at room temperature by PARSTAT 4000 (Princeton Applied Research, USA) electrochemical workstation. The Ni-Co-BH-G deposited NFs were cut into small strips (wires) to use as working electrode in three electrode system, where Pt wire and glassy carbon electrode was used as a counter and a reference electrode, respectively. The electrochemical properties were measured by cyclic voltammtry, galvanostatic charge-discharge and electrochemical impedance spectroscopy (EIS) with 6 (M) KOH electrolyte. The SC values were measured considering the discharging time of the galvanostatic charge-discharge curves according to the equation (2) and (3)

$$SC_S = \frac{I}{\frac{\Delta V}{\Delta t} m} \quad (2)$$

$$SC_C = \frac{I}{\frac{\Delta V}{\Delta t} M} \quad (3)$$

where SC_S and SC_C are corresponding to the three electrode and asymmetric cell, I is the applied current, m is the mass of electro-active material of single electrode in three electrode measurement, M is the total (m_+ and m_-) mass of the electro-active materials in the asymmetric cell, $\Delta V/\Delta t$ is the slope (discharging curve). Energy density (E) and power density (P) of the asymmetric cell based on electro-active materials were calculated by using the equation (4) and (5)

$$E = \frac{1}{2} SC_C \times V^2 \quad (4)$$

$$P = E/\Delta t \quad (5)$$

Where SC_C is the SC of asymmetric device, Δt is the discharging time, V is the operating potential window.

4. Results and Discussions

The morphology and microstructure of Ni-Co-BH-G composites were revealed by the FE-SEM and TEM image analysis. The FE-SEM images are shown in Fig. 1. Interestingly, the different morphological features were obtained by tailoring the initial precursor ratios (Ni to Co ratios). Fig. 1 shows typical FE-SEM images of Ni-Co-BH-G composites along with the pure Ni-Co-BH. The pure Ni-Co-BH particles were agglomerated resulting poor electrochemical performances. The Ni-Co-BH petals were vertically grown over RGO in Ni-Co-BH-G composites. The Ni-Co-BH nano petals were inserted into the RGO sheets in Ni-Co-BH-G1, where the Ni-Co ratio was 1:1. The flower like Ni-Co-BH was developed with well defined electrolyte transportation path in Ni-Co-BH-G2, where the Ni-Co ratio was 1:2. The Ni-Co-BH petals with an average size of ~100-200 nm were scattered over RGO surface forming an easily electrolyte accessible 3D open framework. The flower like structure was destroyed with increasing the Co ratio in Ni-Co-BH-G3. It may be due to the excess amount of $Co(OH)_2$ formation as the Ni-Co ratio increased to 1:3. Therefore, it can be concluded from the high magnification FE-SEM images that the change in Ni-Co ratios significantly influenced the morphology of the Ni-Co-BH-G composites.

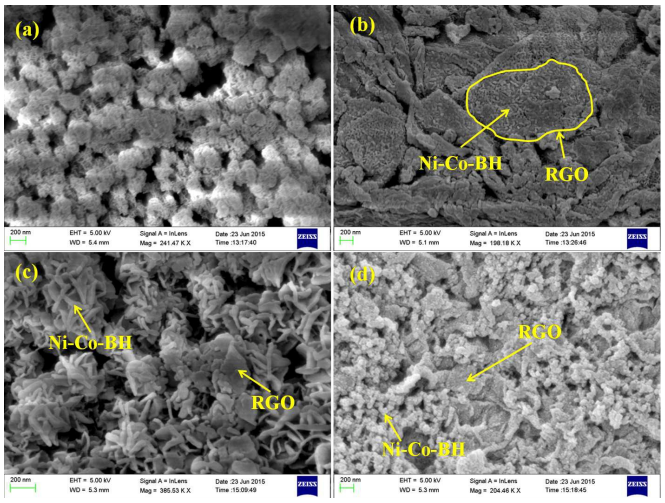

Fig. 1 FE-SEM images of (a) pure Ni-Co-BH, (b) Ni-Co-BH-G1, (c) Ni-Co-BH-G2, and (c) Ni-Co-BH-G3.

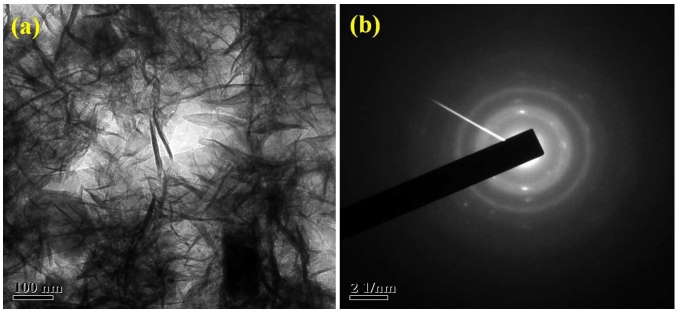

Fig. 2 (a) TEM and (b) SAED pattern images of Ni-Co-BH-G2.

TEM images of Ni-Co-BH-G2 are in line with the observation of FE-SEM image suggesting the lateral dimension of Ni-Co-BH petals in the range of ~100-200 nm (Fig. 2a). Further, these observations confirmed the cross-linking of RGO sheets forming a loosely bounded scaffold like structure with abundant open spaces for the electrolyte to penetrate inside the electrode. The selected area electron diffraction (SAED) pattern image revealed the polycrystalline nature of the Ni-Co-BH-G2 composite formed by the SILAR technique (Fig. 2b).

The growth of thin films over the metallic substrate through SILAR technique followed two kinetic routs. Growth of precursor ions may occurs at the nucleation sites provided by the immersed substrate. In either way, growth of the precursor ions may takes place at the nucleation sites of the colloidal particles (template) which is deposited on the immersed substrate through electrostatic interactions. Herein, GO was deposited over NF due to the unbalanced force resulted from the interaction between NF and oxidative debris present on the GO surfaces. The Ni^{2+} and Co^{2+} ions were adsorbed on the nucleation sites provided by the oxygen functionalities of GO. The Ni^{2+} and Co^{2+} ions were further converted to their respective hydroxides in the basic condition, resulting Ni-Co-BH over the partially reduced GO.[38,39] The Ni-Co-BH further aggregated and crystallized as vertical petals over the RGO surface.[38,39] The SILAR technique followed slow redox reaction at room temperature, which facilitated the slow generation and aggregation of primarily formed Ni-Co-BH to form the flower like Ni-Co-BH-G for the Ni-Co stoichiometric ratio of 1:2. The schematic of formation of Ni-Co-BH-G composite on NF substrate is presented in Fig. 3(a). The digital photograph of the bare NF surface and Ni-Co-BH-G coated substrate is shown in Fig. 3(c, d).

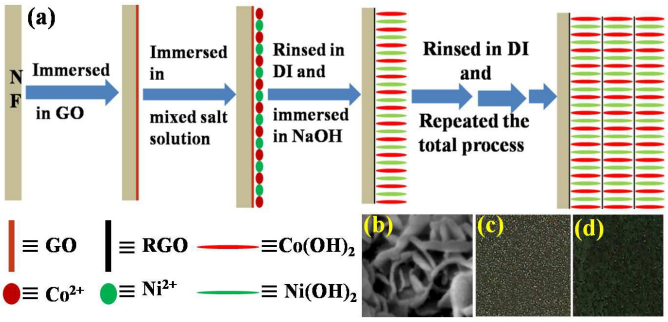

Fig. 3 (a) Shematic representation of Ni-Co-BH-G electrode synthesis by SILAR technique, (b) FE-SEM image of flower like Ni-Co-BH-G2 (c) digital photograph of bare NF and (d) Ni-Co-BH-G coated NF.

CV was analyzed to observe the faradic nature due to the presence of Ni-Co binary hydroxide system in the Ni-Co-BH-G composites (Fig. 4a). The CV curves of the Ni-Co-BH-G composites exhibited two redox couples for two different redox reactions. The Ni phase displayed oxidation at the high voltage potential, whereas the peaks at lower potential corresponded to the Co phase.[40]The peak corresponding to Co phase showed higher current response in comparison to Ni phase in Ni-Co-BH-G3; whereas the peak associated with Ni phase showed high current response in Ni-Co-BH-G1. The peak related to Co phase was shifted to lower potential with increasing the Co content in Ni-Co-BH-G composites. These observations agreed well with the previously reported literature, where Co systems showed lower redox potential in comparison to the Ni systems due to their inbred electrochemical response to the electrolyte.[30,41-43] Therefore, the appearance of two different redox peaks for two different redox environments suggested the successful preparation of Ni-Co-BH-G system taking GO as directing template.[29,30,40]

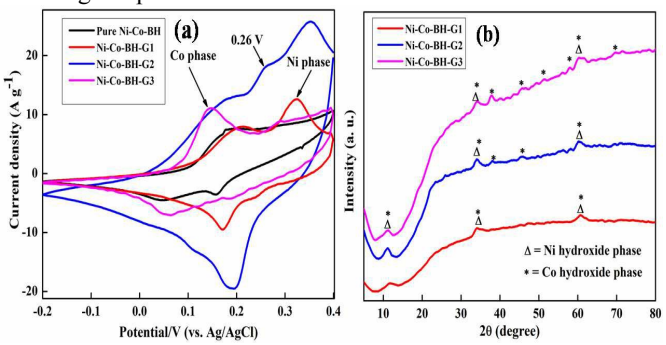

Fig. 4 (a) CV of pure Ni-Co-BH along with Ni-Co-BH-G electrodes in three electrode configuration, (b) XRD pattern of Ni-Co-BH-G.

A broad peak at ~0.26 V appeared in the CV curve of Ni-Co-BH-G2 electrode. This may be due to the presence of multiple phases in Ni-Co-BH-G2.[30] The overlapping of the Ni and Co phase can also provide the intermediate peak, which demonstrated the benefit of the binary systems with more feasible redox states of both metal ions.[30] Formation of Ni-Co-BH-G was investigated by XRD analysis (Fig. 4b). Ni-Co-BH-G1 shows characteristic peaks at 2θ ~11.2 (003), 34.1 (100) and 60.7º (110) corresponding to Ni hydroxide phase.[29,30,40] Interestingly, there was no additional phase for Co hydroxide suggesting the successful incorporation of Co into the single Ni hydroxide phase forming a Ni-Co hydroxide solution (solid).[29,30,40] The XRD pattern of Ni-Co-BH-G2 showed the additional characteristic peaks at 2θ ~37.8 (101) and 45.8º (111) for Co hydroxide phase along with Ni hydroxide and Ni-Co hydroxide intercalated phase.[29,30,40]The peak corresponding to Co hydroxide phase appeared in Ni-Co-BH-G3 with relatively greater intensity. Some more additional peaks at 2θ ~ 51.2 (012), 58.1 (110) and 70º (113) corresponding to Co hydroxide phase has also appeared in the XRD pattern of Ni-Co-BH-G3.[29,30,40] It might be due to the formation of greater amount of Co hydroxide phase as the Co precursor was taken in higher amount in the Ni-Co-BH-G3 composite. The results obtained from the XRD analysis were in line with the observation from FE-SEM and CV analysis. The easily accessible porous framework of the Ni-Co-BH-G composites were also confirmed by the N_2 adsorption-desorption isotherm at 77 K (Fig. S1). The surface area, average pore diameter and pore volume of the Ni-Co-BH-G composites were summarised in Table S1 of supplementary information. Notably, the surface area and pore volume of the composites were changed significantly with their Ni-Co ratios. The ternary system consists of RGO and vertically aligned Ni-Co-BH nano petals expedited the 3D framework with a maximum Brunauer-Emmet-Teller (BET) surface area of 97.05 m^2 g^{-1} for Ni-Co-BH-G2. The flower like Ni-Co-BH provided a 3D building block with an average pore diameter and a pore volume of 3.64 nm and 0.84 cm^3 g^{-1}, respectively for the Ni-Co-BH-G2 composite. Therefore, the high supercapacitor performances of Ni-Co-BH-G2 were expected with its mesoporous conductive network.[22,29,30,33]

XPS of Ni-Co-BH-G2 was explored to investigate the chemical structure of Ni-Co-BH-G composite synthesized by SILAR

method. Typical XPS survey spectra suggested the presence of Ni 2p and Co 2p of Ni-Co-BH along with C 1s spectra of RGO (supplementary Fig. S3) in Ni-Co-BH-G2. Fig. 5(a, b) shows the core level Ni 2p (Ni $2p_{3/2}$ and Ni $2p_{1/2}$) and Co 2p (Co $2p_{3/2}$ and Co $2p_{1/2}$) XPS of the Ni-Co-BH-G2 composite.[2,21,43-45] The deconvoluted Ni 2p and Co 2p peaks can be attributed to the formation of $Ni(OH)_2$ and $Co(OH)_2$ in Ni-Co-BH-G2.[2,21,43-45] The deconvoluted C 1s spectra of Ni-Co-BH-G2 displayed the presence of C=C bonds along with various oxygen functionalities due to the partial reduction of GO in presence of strong base (Fig. 5c).[46,47]

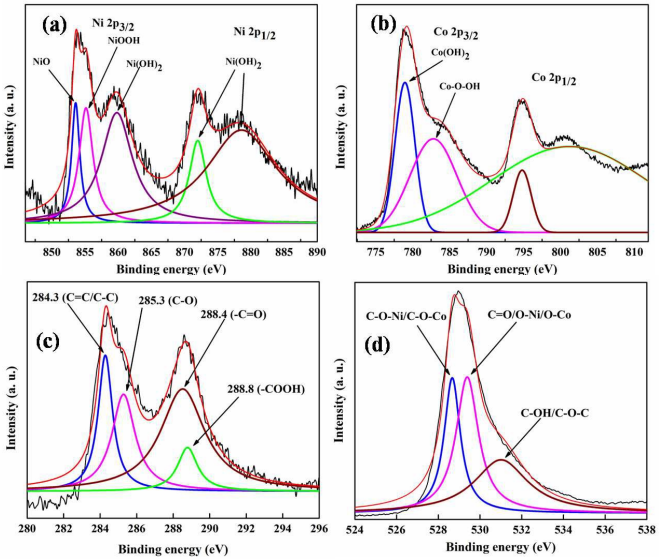

Fig. 5 (a) Ni 2p, (b) Co 2p, (c) C 1s and (d) O 1s XPS spectra of Ni-Co-BH-G2.

The hydrophilic groups of precursor GO played important role in the synthesis of Ni-Co-BH-G composites through the anchoring sites for the adsorption of Ni^{2+} and Co^{2+} followed by the conversion to their metal hydroxide in an alkali medium.[48] On the other hand, the residual oxygen functionalities of partially reduced RGO improved the wettability of the electrode.[48] The deconvoluted O 1s XPS revealed the peaks at 528.6, 529.4 and 531.0 eV related to C-O-Ni/C-O-Co, C=O/O-Ni/O-Co and C-OH/C-O-C, respectively. All these observations confirmed the formation of $Ni(OH)_2$ and $Co(OH)_2$ on the RGO surfaces (Fig. 5d).[50-52] Raman spectra were employed to investigate the chemical environment of RGO and formation of mixed metal hydroxides (Fig. S4). The D and G bands of graphite are attributed to disorder band and in phase vibration of sp^2 hybridised C atoms, respectively.[4,5,32] The D and G bands of GO appeared at ~1335 and 1590 cm^{-1}, respectively due to the incorporation of oxygen functionalities during oxidation of graphite flakes.[4,5,32] The D and G band peaks of the Ni-Co-BH-G composites were appeared at ~ 1350 and 1585 cm^{-1}, respectively. The significant changes in the D and G band peak positions can be ascribed to the restoration of π-electronic conjugation through the de-oxygenation of GO by SILAR method in presence of NaOH.[4,5] The I_D/I_G ratio (intensity ratio of the D band to the G band) can be used to measure the degree of disorder and the presence of residual oxygen functionalities on the RGO surface. The I_D/I_G ratios were calculated to be ~1 for the Ni-Co-BH-G composites, suggesting partial reduction of oxygen functionalities. The appearance of a broad peak at 880 cm^{-1} at the Raman spectrum of Ni-Co-BH-G2 assigned to the formation of β-$Ni(OH)_2$ lattice mode.[38] The appearance of overtone peak at 950 cm^{-1} reflected the poor crystallinity of Ni-Co-BH-G1.[53] The intensive peak at ~660 cm^{-1} signified the A_{1g} symmetry of $Co(OH)_2$ phase in the Ni-Co-BH-G composites.[54] The peaks related to the $Ni(OH)_2$ were absent in the Raman spectrum of Ni-Co-BH-G3, it may be due to the crowded Co^{2+} precursor in the synthetic route of Ni-Co-BH-G3. FT-IR spectra also provided valuable information about the chemical functionalities of the Ni-Co-BH-G composites (Fig. S5). The peaks related to the -OH (~1066 cm^{-1}), epoxy (~1232 cm^{-1}) and -COOH (~1731 cm^{-1}) functionalities of GO were almost absent in the FT-IR spectra of Ni-Co-BH-G composites, suggesting reduction of GO during SILAR technique.[4,5] The metal oxide/hydroxide functionalities were revealed by the appearance of peaks at ~648 and 520 cm^{-1} in the FT-IR spectra of Ni-Co-BH-G composites.[29,45,49] Comparison of electrical conductivity of GO and Ni-Co-BH-G composites can be one of the best techniques to measure the extent of the reduction.[4,5] The presence of sp^3 bonded carbons atoms lowers the electrical conductivity of GO.[4,5] The electrical conductivity can be increased by removing the oxygen functionalities and restoring the conjugated sp^2 network.[4] The electrical conductivity of GO, pure Ni-Co-BH, Ni-Co-BH-G1, Ni-Co-BH-G2 and Ni-Co-BH-G3 were found to be 9.3×10^{-2}, 0.1, 2.1, 4.0 and 1.7 S m^{-1}, respectively. The significant improvement in electrical conductivity of the Ni-Co-BH-G composites confirmed the reduction of GO. The electrical conductivity of the Ni-Co-BH-Gs electrode increased in comparison to the Ni-Co-BH after incorporation of RGO.

The XRD, Raman, FT-IR spectra and electrical conductivity results suggested the mixed metal hydroxides (Ni and Co) were successfully decorated on the RGO template along with the reduction of GO in presence of strong base by the SILAR technique. The deconvoluted C 1s (XPS) spectra of Ni-Co-BH-G2 revealed the presence of some residual oxygen functionalities. So, it can be concluded from the XRD, Raman, FT-IR, XPS spectra and electrical conductivity measurement that the GO was partially reduced to RGO in the Ni-Co-BH-G composites.

Supercapacitor properties of Ni-Co-BH-G composites and pure Ni-Co-BH were analysed with CV, galvanostatic charge-discharges and EIS. The area encircled by the CV curves was improved by incorporating the graphene to the binary hydroxide system (Fig. 4a). Two pairs of redox peaks were associated with two different pseudo reactions provided by the Ni-Co-BH system in 6 (M) KOH electrolyte. The two redox reactions can be described according to the equation (6) & (7).[26]

$$Co(OH)_2 + OH^- \longleftrightarrow Co\text{-}O\text{-}OH + H_2O + e^- \quad (6)$$

$$Ni(OH)_2 + OH^- \longleftrightarrow Ni\text{-}O\text{-}OH + H_2O + e^- \quad (7)$$

The current response of Ni-Co-BH-G2 electrode is higher than other Ni-Co-BH-G electrodes at 10 mV s^{-1}, suggesting that it would be the best material to design the supercapacitor device among the other Ni-Co-BH-G electrodes (Fig. 4a).

The CV of Ni-Co-BH-G electrodes were performed with different sweep rates, ranging from 10-200 mV s^{-1} (Fig. 6). The plot of cathodic peak current density vs. square root of the scan rate showed a straight line for Ni-Co-BH-G2 and Ni-Co-BH-G3 as shown in the supplementary Fig. S6. However, in case of Ni-Co-BH, the cathodic peak current density vs. square root of the

scan rate plot was not fitted well with a straight line. The slope (i.e., cathodic peak current response) of pure Ni-Co-BH was found to be 1.66 and increased to 4.14 for Ni-Co-BH-G1. Interestingly, current response increased linearly with the square roots of the scan rates for even high scan rate of 100 mV s^{-1} and the slopes were found to be 8.82 and 9.06 for Ni-Co-BH-G2 and Ni-Co-BH-G3, respectively. The increased slope of the well fitted cathodic peak current density vs. square root of the scan rate plots for Ni-Co-BH-G2 and Ni-Co-BH-G3 suggested relatively rapid charge transfer process at the electrode-electrolyte interfaces for the Ni-Co-BH-G2 and Ni-Co-BH-G3 electrodes in compare to Ni-Co-BH and Ni-Co-BH-G1.[55-56] The inadequately fitted cathodic peak current density vs. square root of the scan rate plot with poor slope values suggested that the diffusion of ions was not compatible with the transport of electrons through the external circuits at high scan rates for the Ni-Co-BH and Co-BH-G1 electrodes.[55-56] It is seen that the Ni-Co-BH-G2 and Ni-Co-BH-G3 exhibited more than 2 times faster electrolyte diffusion than Ni-Co-BH-G1 electrode. These results suggested that Ni-Co-BH-G2 and Ni-Co-BH-G3 electrodes exhibited fast and efficient ion diffusion, which may be due intrinsic morphology and electrical conductivity properties of the composite.[55-56] The galvanostatic charge-discharge curves of Ni-Co-BH-G electrodes were measured at different current densities (supplementary Fig. S7). The non linear charge-discharge curves obtained for all the Ni-Co-BH-G composite electrodes supported the XRD, XPS, FT-IR and CV results.

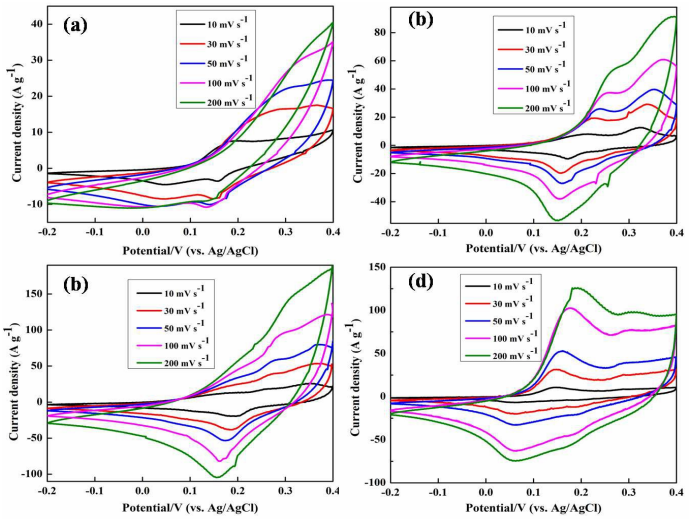

Fig. 6 CV curves of (a) pure Ni-Co-BH, (b) Ni-Co-BH-G1, (c) Ni-Co-BH-G2, and (c) Ni-Co-BH-G3.

The SC_S values were evaluated from the discharge curves of charge-discharges cycle. The SC_S was found to be 678 F g^{-1} at a current density of 2 A g^{-1} for pure Ni-Co-BH, which was decreased to 148 F g^{-1} at a current density of 10 A g^{-1}. The SC_S was increased to 1.5-2 times after the introduction of RGO in Ni-Co-BH-G composites. GO served as directing template providing nucleation sites for the metal ions to decorate Ni-Co-BH without agglomeration resulting better electrolyte penetration as evidenced from the FE-SEM and TEM image analysis. The RGO also improved the electrical conductivity of the Ni-Co-BH-G composites, which might reduce the solution resistance of the supercapacitor electrode. The superior supercapacitor performances of the Ni-Co-BH-G composites as compared to the pure Ni-Co-BH are attributed to the synergistic effect of RGO and Ni-Co-BH systems present in the composites. The SC_S of Ni-Co-BH-G electrodes changed with their different Ni-Co compositions in a wide range of current densities from 2-10 A g^{-1}. The SC_S values increased with increasing the concentration of Co^{2+} (from Ni-Co-BH-G1 to Ni-Co-BH-G2) with a given concentration of Ni^{2+}. Further increasing the concentration of Co^{2+} ions in the "SILAR" solution resulted lower SC_S in Ni-Co-BH-G3 as compared to Ni-Co-BH-G2. The supercapacitor properties of the Ni-Co-BH-G electrodes perhaps associated to their compositions as well as distinctive morphologies. The excellent SC_S of 2130 F g^{-1} at 2 A g^{-1} provided by Ni-Co-BH-G2 is the highest among the rest of the Ni-Co-BH-G composites. It is seen that the SC_S values decreased with increasing current density as summarized in Fig. 7 (a). The outer surface of the electrode materials is available only for electrolyte access, leaving dead region in the bulk position due to the limited diffusion of electrolyte ions at high current density. Notably, the Ni-Co-BH-G electrodes prepared by a facile SILAR method exhibited fast charge-discharge performance with high rate potential. The retention of SC_S values were 20, 20, 49 and 58% for pure Ni-Co-BH, Ni-Co-BH-G1, Ni-Co-BH-G2 and Ni-Co-BH-G3, respectively. Retention trend of SC_S with increasing current density values fully supported the results obtained from the CV curves (cathodic current density slope).

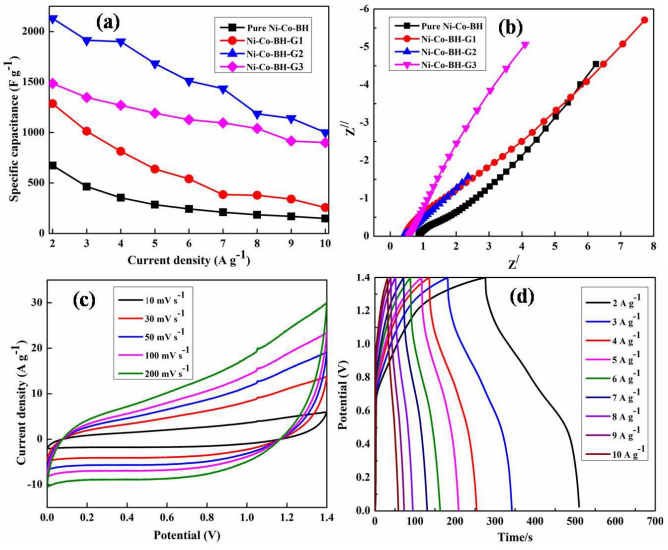

Fig. 7 (a) SC_S vs. current density plots (b) Nyquist plot of pure Ni-Co-BH and Ni-Co-BH-G electrodes (c) CV at various scan rates ranging from 10-200 mV s^{-1} (d) galvanostatic charge-discharge curves at various current densities of 2-10 A g^{-1} of Ni-Co-BH-G2//CCN asymmetric device.

Interestingly, Ni-Co-BH-G2 provided lower rate capability than that of Ni-Co-BH-G3, but, showed better SC_S at a current density of 10 A g^{-1}.

EIS of the samples were recorded to observe the variation of supercapacitor properties with different compositions, which were obtained from the CV and galvanostatic charge-discharge curves. The EIS curves were fitted with a Randles circuit involving series resistance (Rs) and charge-transfer resistance (Rct), constant phase element (CPE), and a Warburg element (W) (Fig. 7b).[57-62] The CPE of the Nyquist plot can be

expressed by two physical terms, CPE-T and CPE-P. CPE-T is associated with the double layer capacitance of the active materials, whereas CPE-P can be ascribed to the capacitive nature of the charge-transfer path.[57-62] The W, which is associated with the ion diffusion route can also be deconvoluted into 3 parts: resistance (W-R), diffusion time constant (W-T) and the exponent (W-P) determining the capacitive nature of the electrolyte diffusion.[57-63] All the Randles circuit related values were simulated by using Z-View software (supplementary Fig. S8) and presented in Table 1. The Rs values were fully supported by the electrical conductivity results of the pure Ni-Co-BH and Ni-Co-BHG composites. The Ni-Co-BH-G2 provided good Rs (0.37 Ω), Rct (0.5), CPE-T (0.22), CPE-P (0.5), W-R (9 Ω), W-T (0.3) and W-P (0.45) values suggesting superior electrochemical performances among the Ni-Co-BH-G composites. Interestingly, it can be noted that the W-T values were comparable with the cathodic peak current slope obtained from the CV curves. The Ni-Co-BH-G3 provided better W-T (0.26) value than Ni-Co-BH-G2 (0.30), signifying faster electrolyte ion diffusion in Ni-Co-BH-G3 than Ni-Co-BH-G2 electrode as the cathodic peak current slope and retention of SC_S plots suggested. The lower SC_S values of Ni-Co-BH-G3 than Ni-Co-BH-G2 may be due to the poor electrical conductivity, Rs, Rct, CPE-T, CPE-P, W-R and lower surface area of Ni-Co-BH-G3 in comparison to Ni-Co-BH-G2.

CV, charge-discharge, EIS and electrical conductivity analysis confirmed that the Ni-Co-BH-G2 is the ideal material for supercapacitor applications among the studied Ni-Co-BH-G composites. The superior supercapacitor property of Ni-Co-BH-G2 electrodes is attributed to its high electrical conductivity (4.0 S m^{-1}) ensuring low contact resistance. In addition, the vertically aligned Ni-Co-B-H petals grown on the RGO surface resulted meso porous (3.64 nm) network with high surface area of 97.05 m^2 g^{-1} over the macro porous NF. The superlative 3D porous platform allowed superficial electrolyte access for reversible and fast pseudo-reaction without any blockage of binders. Overall, the fabrication of 3-D electrodes by a facile, simple and low cost SILAR method gains superior benefits in designing supercapacitor devices. In order to further investigate the supercapacitor properties towards the practical applications an asymmetric device (Ni-Co-BH-G2//CCN) was engineered with the Ni-Co-BH-G2 as positive electrode and CCN as the negative electrode. The CV curves of CCN displayed a quasi-rectangular shape in the potential window of 0.1-1 V, signifying fast ion transport of electrolyte and the EDL nature of CCN electrode (Fig. S10). The mass balancing of the electrode materials was carried out from supplementary Fig. S11 of supporting information according to the equation (8)[3]

$$\frac{m_+}{m_-} = \frac{\Delta V_- \times SC_-}{\Delta V_+ \times SC_+} \qquad (8)$$

Where, m is the mass, ΔV is the voltage window, SC is the specific capacitance of positive (+) and negative (-) electrodes, respectively. The mass ratio of CCN to Ni-Co-BH-G2 was measured to be ~1.5:1. The total mass of the active materials was ~2.5 mg. Unlike the sharp pseudo peaks exhibited in the CV curves of the Ni-Co-BH-G2 electrode, the Ni-Co-BH-G2//CCN asymmetric device provided a nearly rectangular CV in the potential window of 0-1.4 V, signifying distinctive supercapacitor activities (Fig. 7c). This typical behaviour was rarely experienced with metal hydroxide based asymmetric devices.[1] The charge-discharge curves of the asymmetric device were not perfectly straight line, which signified the involvement of redox nature with EDLC. The SC_C values were found to be 340, 336, 333, 327, 313, 291, 244, 213, 194 F g^{-1} at current densities of 2, 3, 4, 5, 6, 7, 8, 9, 10 A g^{-1}, respectively. About 96% of its initial SC_C was retained when the current density increased from 2 to 5 A g^{-1}. The Ragone plot is shown in Fig. 8 (b). Ni-Co-BH-G2//CCN experienced a very high energy density of ~92 W h kg^{-1} at a power density of 1.4 kW kg^{-1}. The energy density was found to be ~52.9 W h kg^{-1} at very high power density of ~7.0 kW kg^{-1} for the Ni-Co-BH-G2//CCN supercapacitor device. EIS of the Ni-Co-BH-G2//CCN device was also conducted to observe the electrochemical characteristics according to the Randles circuit (Fig. 8c). The Nyquist plot of the device was fitted with Z-View software (Fig. S12) and the corresponding values are shown in Table 1. The very low Rs (0.22 Ω), Rct (1.5 Ω), W-R (1.0 Ω) and comparable CPE values facilitated to exhibit the excellent supercapacitor behaviour of the Ni-Co-BH-G2//CCN supercapacitor device. The slight increase of Rct in Ni-Co-BH-G2//CCN than that of Ni-Co-BH-G2 can be due to the combination of two different charge transfer processes provided by two different electrodes. The improved CPE-P and W-P values for the supercapacitor device as compared to the single electrodes may be due to the hybridisation with CCN (conducting).

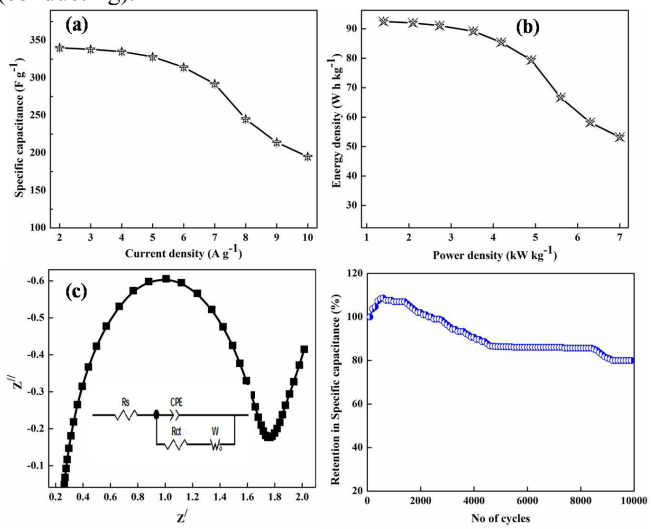

Fig. 8 (a) SC_C vs. current density (b) Ragone (c) Nyquist plot and (d) stability curve up to 10,000 cycles of Ni-Co-BH-G2//CCN asymmetric device.

These excellent supercapacitor values of the asymmetric device are superior or comparable to the other metal hydroxide and binary hydroxide based electrodes.[29-31,36,37,56-61] Finally, an elongated life span is an essential requirement for any kind of energy storage device. Long life cycle of Ni-Co-BH-G2//CCN was experienced by repeating charge-discharge tests at a current density of 10 A g^{-1} for 10,000 cycles. The SCs retention of the Ni-Co-BH-G2//CCN device as a function of charge-discharge cycles is shown in Fig. 8(d). It was worth noting that the SCs was increased initially up to 500 cycles, which was probably due to the wetting of the electrode by KOH and surface activation of the electro-active materials. The SCs started to decrease gradually after 500 cycles and retained ~87% after 4000 cycles. After 10,000 cycles the retention was ~80%. The outstanding cyclic stability of the Ni-Co-BH-G2//CCN device confirmed the exact hybridization of positive

and negative electrode materials. In order to verify the practical application four Ni-Co-BH-G2//CCN devices were assembled in a series. The assembled system provided ~5.6 V charge-discharge potential. The assembled system has powered a 5 V light-emitting diode (LED) successfully.

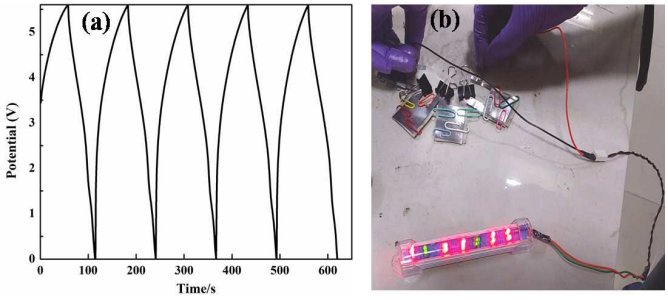

Fig. 9 (a) Galvanostatic charge-discharge curves of four Ni-Co-BH-G2//CCN asymmetric devices connected in a series (b) An LED indicator powered by the four assembled devices.

5. Conclusions

The controllable SILAR technique to prepare Ni-Co-BH-G electrode has number of advantages over the conventional procedure of metal binary hydroxide preparation. The SILAR method provided a binder-free route to prepare supercapacitor electrode of Ni-Co-BH-G on NF substrate through a cost-effective, less time consuming and eco-friendly path to avoid the dead surface of the conventional electrode preparing technique. The oxidative debris of GO provided anchoring sites to the precursor materials to adsorb the Ni^{2+} and Co^{2+} followed by the conversion to their metal hydroxide in an alkali medium. The hydrophilic groups of the partially reduced RGO improved the wettability of the electrode. The RGO also enhanced the electrical conductivity of the Ni-Co-BH-G composites, which might reduce the solution resistance of the Ni-Co-BH-G composites. The EDLC of RGO and pseudocapacitance of Ni-Co-BH simultaneously improved the electrochemical properties of the Ni-Co-BH-G composites. Different morphological features were obtained for the Ni-Co-BH-G composites by changing the initial precursor (Ni to Co ratios) ratios. The flower like Ni-Co-BH petals grown over RGO surface provided high surface area of 97.05 m^2 g^{-1}, average pore diameter of 3.64 nm, pore volume of 0.84 cm^3 g^{-1} and electrical conductivity of 4.0 S m^{-1} for the Ni-Co-BH-G2 composite. The Ni-Co-BH petals with consistent RGO nano sheets arrays over conductive macro porous NF served as an outstanding 3-D electrode, showing SC_S of 2130 F g^{-1} at 2 A g^{-1} and low solution resistance. The cathodic peak current density vs. square root of the scan rate slope values suggested the high rate capability of the Ni-Co-BH-G2 electrode, which was further supported by the SC_S and W-T values obtained from the charge-discharge curves and Nyquist plot, respectively. Furthermore, an asymmetric device (Ni-Co-BH-G2//CCN) was engineered with the optimized Ni-Co-BH-G arrays as positive electrode and CCN as a negative electrode. The designed device demonstrated outstanding supercapacitor properties with high SC_C (340 F g^{-1}), energy density (~92 W h kg^{-1}), power density (~7.0 kW kg^{-1}) and long cyclic durability. The excellent supercapacitor performance of Ni-Co-BH-G2 composite electrode suggested that the scalable SILAR method has enormous prospective in various energy storage technologies.

s

Acknowledgements

Authors are thankful to the Director of CSIR-CMERI. Authors are also thankful to the Department of Science and Technology, New Delhi, India, for the financial support from the DST-INSPIRE Faculty Scheme - INSPIRE Programme (IFA12CH-47) and Council of Scientific and Industrial Research, New Delhi, India, for funding MEGA Institutional project (ESC0112/RP-II). This study was also supported by the fund from the ministry of South Korea (2014M3C1A8054240).

Notes and references

[a] *Surface Engineering & Tribology Division, Council of Scientific and Industrial Research-Central Mechanical Engineering Research Institute, Durgapur -713209, India*
[b] *Academy of Scientific and Innovative Research (AcSIR), CSIR-CMERI Campus, Durgapur-713209, India*

[c] *Department of BIN Conversion Technology, Chonbuk NationalUniversity, Jeonju, Jeonbuk 561-756, Republic of Korea*

*Correspondence to: Dr. Tapas Kuila (E-mail: tkuila@gmail.com; Phone: +919647205077) and Prof. Joong Hee Lee (E-mail: jhl@chonbuk.ac.kr; Phone: +82632702342)

References

1 Z. Tang, C. Tang and H. Gong, *Adv. Funct. Mater.*, 2012, **22**, 1272.
2 D. P. Dubal, R. Holze and P. G. Romero, *Sci. rep.*, 2014, **4**, 7349.
3 W. Chen, C. Xia, and H. N. Alshareef, *ACS nano*, 2014, **8**, 9531.
4 M. Jana, S. Saha, P. Samanta, N. C. Murmu, J. H. Lee and T. Kuila, *Mater. Chem. Phys.*, 2015, **151**, 72.
5 M. Jana, P. Khanra, N. C. Murmu, P. Samanta, J. H. Lee and T. Kuila, *Phys. Chem. Chem. Phys.*, 2014, **16**, 7618.
6 P. Simon and Y. Gogotsi, *Nat. Mater.*, 2008, **7**, 845.
7 E. Frackowiak, *Phys. Chem. Chem. Phys.*, 2007, **9**, 1774.
8 D. N. Futaba, K. Hata, T. Yamada, T. Hiraoka, Y. Hayamizu, Y. Kakudate, O. Tanaike, H. Hatori, M. Yumura and S. Iijima, *Nat. Mater.*, 2006, **5**, 987.
9 A. G. Pandolfo and A. F. Hollenkamp, *J. Power Sources*, 2006, **157**, 11.
10 X. Lang, A. Hirata, T. Fujita and M. Chen, *Nat. Nanotechnol.*, 2011, **6**, 232.
11 S.-M. Chen, R. Ramachandran, V. Man and R. Saraswathi, *Int. J. Electrochem. Sci.*, 2014, **9**, 4072.
12 Z. Yu, L. Tetard, L. Zhai and J. Thomas, *Energy Environ. Sci.*, 2015, **8**, 702.
13 J. Chmiola, G. Yushin, Y. Gogotsi, C. Portet, P. Simon and P. L. Taberna, *Science*, 2006, **313**, 1760.
14 J. Lee, J. Kim and T. Hyeon, *Adv. Mater.*, 2006, **18**, 2073.

15 E. Frackowiak and F. Beguin, *Carbon*, 2002, **40**, 1775.
16 P. J. Hall, M. Mirzaeian, S. I. Fletcher, F. B. Sillars, A. J. R. Rennie, G. O. S. Bey, G. Wilson, A. Cruden and R. Carter, *Energy Environ. Sci*., 2010, **3**, 1238.
17 J. Jiang, Y. Li, J. Liu, X. Huang, C. Yuan and X. W. Lou, *Adv. Mater*., 2012, **24**, 5166.
18 W. Wei, X. Cui, W. Chen and D. G. Ivey, *Chem. Soc. Rev.*, 2011, **40**, 1697.
19 G. A. Snook, P. Kao and A. S. Best, *J. Power Sources*, 2011, **196**, 1.
20 R. B. Rakhi, W. Chen, D. Cha and H. N. Alshareef, *Nano Lett*., 2012, **12**, 2559.
21 C.-T. Hsu and C.-C. Hu, *J. Power Sources*, 2013, **242**, 662.
22 R. Wang and X. Yan, *Sci. Rep*., 2014, **4**, 3712.
23 X. Yu, B. Lu and Z. Xu, *Adv. Mate*r., 2014, **26**, 1044.
24 R. S. Jayashree, P. V. Kamath and G. N. Subbanna, *J. Electrochem. Soc*., 2000, **147**, 2029.
25 Z. Zhang, K. Chi, F. Xiao and S. Wang, J. Mater. Chem. A, 2015, 3, 12828.
26 Z. Zhang, F. Xiao and S. Wang, J. Mater. Chem. A, 2015, 3, 11215.
27 Z. Zhang, F. Xiao , L. Qian, J. Xiao, S. Wang, and Y. Liu, Adv. Energy Mater., 2014, 4, 00064.
28 X. Sun, G. K. Wang, J. Y. Hwang and J. Lian, *J. Mater. Chem*., 2011, **21**, 16581.
29 Y. Tang, Y. Liu, W. Guo, S. Yu and F. Gao, *Ionics*, 2015, **21**, 1655.
30 X. Sun, G. Wang, H. Sun, F. Lu, M. Yu and J. Lian, *J. Power Sources*, 2013, **238**, 150.
31 X. Wang, A. Sumboja, M. Lin, J. Yan and P. S. Lee, *Nanoscale*, 2012, **4**, 7266.
32 M. Jana, S. Saha, P. Samanta, N. C. Murmu, N. H. Kim, T. Kuila and J. H. Lee, *Nanotechnology*, 2015, **26**, 075402.
33 G. S. Gund, D. P. Dubal, S. S. Shinde and C. D. Lokhande, *ACS Appl. Mater. Interfaces*, 2014, **6**, 3176.
34 G. S. Gund, D. P. Dubal, B. H. Patil, S. S. Shinde and C. D. Lokhande, *Electrochim. Acta*, 2013, **92**, 205.
35 G. S. Gund, D. P. Dubal, S. B. Jambure, S. S. Shinde and C. D. Lokhande, *J. Mater. Chem. A*, 2013, **1**, 4793.
36 U. M. Patil, J. S. Sohn, S. B. Kulkarni, S. C. Lee, H. G. Park, K. V. Gurav, J. H. Kim and S. C. Jun, *ACS Appl. Mater. Interfaces*, 2014, **6**, 2450.
37 Y. Bai, W. Wang, R. Wang, J. Sun and L. Gao, *J. Mater. Chem. A*, 2015, **3**, 12530.
38 D. S. Hall, D. J. Lockwood and C. Bock, *Proc. R. Soc. A*, 2014, **471**, 792.
39 J. W. Lee, J. M. Ko and J.-D. Kim, *J. Phys. Chem. C*, 2011, **115**, 19445.
40 J. Xiao and S. Yang, *RSC Adv.*, 2011, **1**, 588.
41 L. Cao, F. Xu, Y. Y. Liang and H. L. Li, *Adv. Mater*., 2004, **16**, 1853.
42 H. L. Wang, H. S. Casalongue, , Y. Y. Liang and H. J. Dai, *J. Am. Chem. Soc*., 2010, **132**, 7472.
43 S. C. Petitto, E. M. Marsh, G. A. Carson and M. A. *J. Mol. Catal. A: Chem.*, 2008, **281**, 49.
44 J. Ma, T. Yuan, Y.-S. He, J. Wang, W. Zhang, D. Yang, X.-Z. Liao and Z.-F. Ma, J. Mater. Chem. A, 2014, 2, 16925.
45 P. Prieto, V. Nistor, K. Nouneh, M. Oyama, M. A. Lefdil and R. Díaz, *Appl. Surf. Sci*., 2012, **258**, 8807.
46 X. Fan, W. Peng, Y. Li, X. Li, S. Wang, G. Zhang, and F. Zhang, Adv. Mater., 2008, 20, 4490.
47 J. P. Rourke, P. A. Pandey, J. J. Moore, M. Bates, I. A. Kinloch, R. J. Young, and N. R. Wilson, Angew. Chem. Int. Ed., 2011, 50, 3173.
48 N. V. Kosova, E. T. Devyatkina and V. Kaiche, *J. Power Sources*, 2007, **174**, 735.
49 S. Tardio, M.-L. Abel, R. Carr, J. E. Castle and J. F. Watts, J. Vac. Sci. Technol. A, 2015, 33, 05E122.
50 H. Xie, S. Tang, Z. Gong, S. Vongehr, F. Fang, M. Li and X. Meng, *RSC Adv*., 2014, **4**, 61753.
51 M. C. Biesinger, B. P. Payne and L. W. M. Lau, *Surf. Interface Anal*., 2009, **41**, 324.
52 J. E. Castle, J. Adhes., 2008, 84, 368.
53 J. R. Neilson, B. Schwenzer, R. Seshadri and D. E. Morse, *Inorg. Chem*., 2009, **48**, 11017.
54 H. B. Li, Y. Q. Gao and G. W. Yang, *RSC Adv*., 2015, **5**, 45359.
55 T. W. Lin, C. S. Dai and K. C Hung, *Sci. Rep*., 2014, **4**, 7274.
56 A. Arslan and E. Hür, Int. *J. Electrochem. Sci*., 2012, **7**, 12558.
57 B. X. Fan, W. Peng, Y. Li, X. Li, S. Wang, G. Zhang, and F. Zhang, *Adv. Mater*., 2008, **20**, 4490.
58 M. Jana, S. Saha, P. Khanra, P. Samanta, H. Koo, N. C. Murmu and T. Kuila, *J. Mater. Chem. A*, 2015, **3**, 7323.
59 L. Oakes, A. Westover, J. W. Mares, S. Chatterjee, W. R. Erwin, R. Bardhan, S. M. Weiss and C. L. Pint, *Sci. Rep*., 2013, **3**, 3020.
60 N. Zhu, W. Liu, M. Xue, Z. Xie, D. Zhao, M. Zhang, J.Chen and T. Cao, *Electrochim. Acta*, 2010, **55**, 5813.
61 J. Song and M. Z. Bazant, *J. Electrochem. Soc*., 2013, **160**, A15.
62 A. Ehsani, M. G. Mahjani, M. Jafarian, *T. J. Chem*. 2011, **35**, 735.
63 M. Y. Ho, P. S. Khiew, D. Isa, T. K. Tan, W. S. Chiu, C. H. Chia, M. A. A. Hamid and R. Shamsudin, *Sains Malays*., 2014, **43**, 885.

Table 1. Z-view fitted values of Rs, Rct, CPE-T, CPE-R, W-R, W-T, W-P from the equivalent circuit corresponded to Fig. S8.

Sample	Rs	CPE-T	CPE-P	Rct	W-R	W-T	W-P
Ni-Co-BH	0.78	0.009	0.43	2.1	36	0.62	0.44
Ni-Co-BH-G1	0.40	0.018	0.61	1.9	10	0.54	0.40
Ni-Co-BH-G2	0.37	0.022	0.52	0.5	9	0.30	0.45
Ni-Co-BH-G3	0.55	0.019	0.75	1.1	22	0.26	0.33

Table of Contents

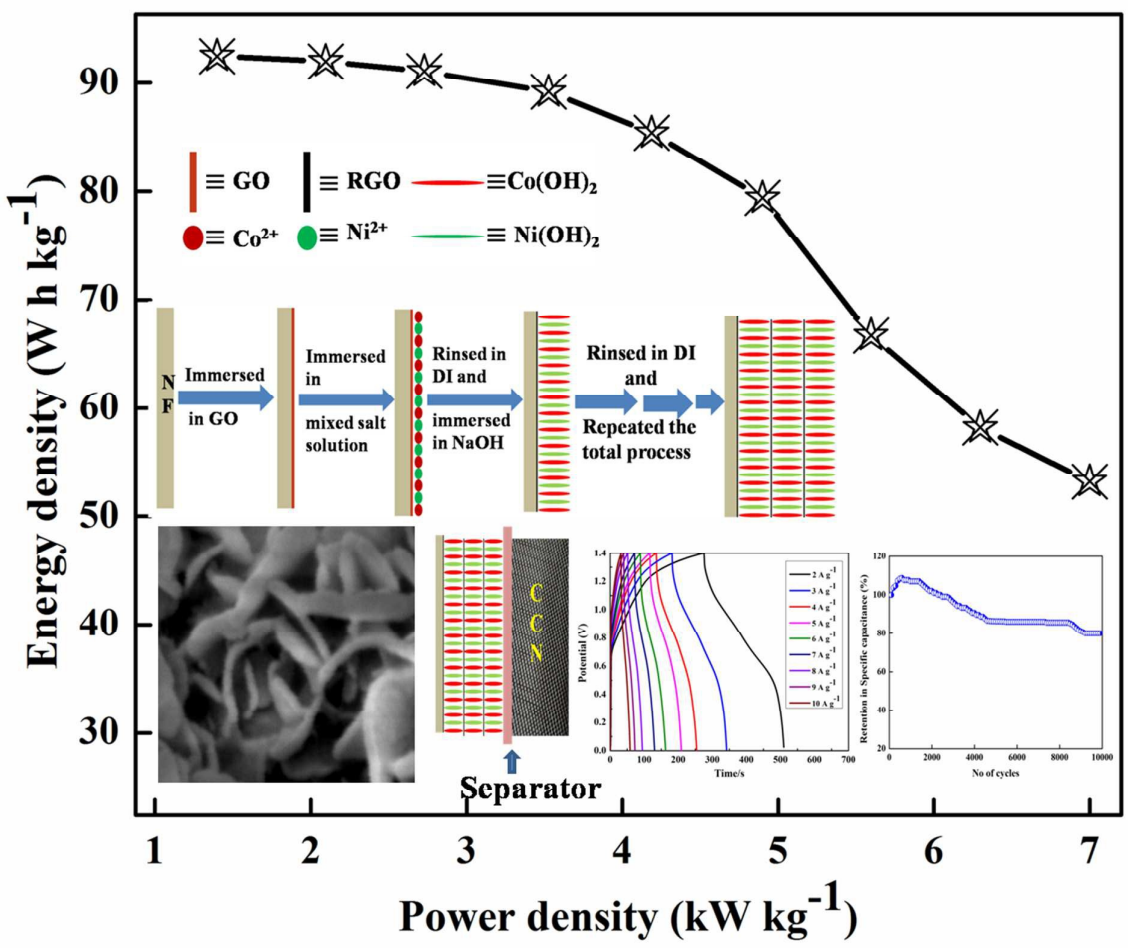

Ni-Co-BH-G was prepared by SILAR technique and the corresponding asymmetric supercapacitor showed the energy density of 92 W h kg^{-1}.